CrossMark

RESEARCH ARTICLE - SYSTEMS ENGINEERING

# A Simple Remote Sensing Ground Receiving System for Interest Creation in Systems Engineering and Geophysics Research

**Abdelatif Hassini[1]** · **Ahmed Hafid Belbachir[2]**

**Abstract** The METEOSAT Second Generation (MSG3) geostationary satellite main payload is the optical imaging radiometer, the so-called Spinning Enhanced Visible and InfraRed Imager (SEVIRI). With its 12 spectral channels and its high temporal resolution, SEVIRI can offer improved geophysics thematic products measurements. So, the development of a system that can exploit the temporal behavior of the terrestrial disk observations is crucial for these near-real-time applications. Advanced Very High Resolution Radiometer (AVHRR) data from polar-orbiting NOAA19 satellite are acquired and processed here. A ground station is required to collect and follow the temporal, spectral, and space evolution of the treated topic of interest. The main objective of this research is to give the most important directives for developing a simple remote sensing ground station. The system consists of hardware and software parts and gives meaningful results using received daily data from either SEVIRI-MSG3 or AVHRR-NOAA19. Satellite multi-sensor database is created and enriched everyday. A realized auto-tracker capable of automatic tracking satellites is mounted in our ground station. Based on received images, some acquisition and MSGViewer software processing results such as brightness temperature, Albedo conversions from the raw data, and different red–green–blue combinations between visible and infrared windows are illustrated and discussed. The system can be easily applied for operational research uses.

**Keywords** Satellite · Sensors · Acquisition · Images · Realization · RGB combination

## 1 Introduction

Remote sensing data are potentially useful source of soil, sea, and atmosphere cover information and can be applied to look at changes in terrestrial Earth globe including the estimation of land cover information [1,2], global and diffuse solar radiation through the terrestrial atmosphere [3], and terrestrial tectonic plates movement evaluation [4].

Satellite images reception technique evolved quickly this last decade. At the first time, the operation required considerable financial means and was therefore limited to specializing organizations. Today, the technique has become more familiar and easier thanks to microcomputer use.

The second of the new generation of METEOSAT satellites, known as METEOSAT Second Generation (MSG3), was launched in July 05, 2012. As with the current METEOSAT series, MSG3 is spin-stabilized and capable of greatly enhanced Earth observations. The satellite's 12-channels imager, known formally as the Spinning Enhanced in Visible and InfraRed Imager (SEVIRI), observes the full disk of the Earth with an unprecedented repeat cycle of 15 min in 12 spectral wavelength regions or channels [5]. High Rate Image Transmission (HRIT) format is used in each image channel.

The NOAA19 Polar Orbiting Environmental Satellite system (POES) was launched in February 06, 2009, and

✉ Abdelatif Hassini
abdelatif_hassini@yahoo.com;
hassini.abdelatif@univ-oran.dz

Ahmed Hafid Belbachir
ahmedhafidbelbachir@gmail.com

[1] Département de Maintenance en Instrumentation, Institut de Maintenance et Sécurité Industrielle, Université d'Oran 2 Mohamed Ben Ahmed, BP 1524, El M'Nouar, Oran, Algeria

[2] Laboratoire d'Analyse et d'Application des Rayonnements, Faculté de Physique, Université USTOMB, BP 1505, El M'Nouar, Bir El Djir, Oran, Algeria

Springer

equipped by an Advanced Very High Resolution Radiometer (AVHRR version 3). It provides remote sensing data in five wavelength bands and tow full spatial resolutions, Automatic Picture Transmission (APT) and High Resolution Picture Transmission (HRPT), the first one is approximately 4 km, the second one is approximately 1 km pixels. These data sets can be used for a variety of remote sensing geophysical applications.

The spacecraft was launched to provide a polar-orbiting platform to support environmental monitoring instruments for imaging and measuring the Earth's atmosphere. It can also cover globe surface, clouds, the Earth's radiation, atmospheric ozone, aerosol distribution, sea surface temperature, vertical temperature, and troposphere and stratosphere water profiles. Measurement of proton and electron flux at orbit altitude, data collection from remote platforms, and the Search and Rescue Satellite-Aided Tracking (SARSAT) system are equally covered.

In this research, we have developed satellite images reception ground station. Data of the images are daily captured with a feed horn motorized system and image processing equipment. The images concern a large identified user community and have expressed the need for information tools operating on environment. Applications are numerous such as coastal protection, climate and meteorology, security, tourism and leisure, fishing and aquaculture, sea traffic, and others domains [6,7]. This project is actually operational and used like a practical work in teaching module of Remote Sensing (Master 2 degree in Radiology Science and Imagery, Faculty of Physics, University USTOMB, Oran, Algeria).

Our effort did not stop at this stage; we applied some techniques of image processing (such as the geometrical correction and the localization of the borders) to facilitate the interpretation of the results of reception. Some thematic products are extracted by using RGB combination method. The reception with high spectral, spatial, and temporal resolutions such as METEOSAT Third Generation (MTG) for our team is a possible operation and remains our prospect.

## 2 Materials and Methods

### 2.1 SEVIRI Sensor

SEVIRI sensor embedded on MSG3 Satellite is a 50-cm-diameter aperture, line-byline scanning radiometer, which provides image data in four Visible and Near-InfraRed (VNIR) channels and eight InfraRed (IR) channels. A key feature of this imaging instrument is its continuous imaging of the Earth in 12 spectral channels with a baseline repeat cycle of 15 min. The imaging sampling distance is 3 km at the sub-satellite point for standard eleven HRIT channels, and down to 1 km for the High Resolution Visible (HRV)

channel. The main characteristics of the instrument are summarized in Table 1.

The primary mission of the MSG3 is the continuous observation of the Earth's full disk with a multi-spectral imager. The high repeat cycle for full-disk imaging provides multi-spectral observations of rapidly changing phenomena such as forest fires, cyclones, deep convection, and others. It also provides for better retrieval of wind fields, which are obtained from the tracking of clouds, water vapor, and ozone features [8]. Change detection is the process of identifying changes that take place in a time series (i.e., through time). The analysis of change detection is implemented by using multi-date imageries [9].

### 2.2 AVHRR/3 Sensor

The POES program includes the last two series. Five NOAA satellites are currently operational. The last one, NOAA19, was launched in February 2009.

NOAA maintains at least two operational satellites in complementary orbits, with the even-numbered satellites crossing the equator in the early morning and early evening and the odd-numbered satellites crossing the equator in the afternoon and late evening. Together they provide twice-daily global coverage and ensure that data for any region of the Earth are no more than 6 h old.

NOAA satellites allow monitoring, on a global scale, snow and sea ice extents, water surface temperatures, or vertical profiles of atmospheric temperature and humidity.

The main sensor package on the POES NOAA satellites is the AVHRR. This sensor gathers data in five different wavelength regions; Table 2 shows some characteristics of the AVHRR/3 radiometer. The bands range covered some parts from visible to thermal infrared radiation. These data are broadcast continually from each satellite as HRPT data in the microwave frequency range and can be received on the ground station during the times that the satellite is visible above the horizon. The maximum pass time (time of image acquisition) is usually 15 min. The data can also be stored on board the satellite on tape recorders for later playback. In the AVHRR/3 version used since NOAA14 satellite, there are six channels [10,11].

The Scanning Radiometer AVHRR is characterized by a very wide field of view. Its swath is 2940 km, and its spatial resolution is approximately 1 km at the sub-satellite point. Instantaneous Field of View (IFoV) of each channel is approximately 1.4 mrad leading to a resolution at the satellite subpoint of approximately 1 km for a nominal altitude of 833 km. The scanning rate of the AVHRR is 360 scans per minute.

The analog data output from the sensors is digitized on board the satellite with 10 bit resolution at a rate of 39.936 samples per second per channel. Each sample step corre-

**Table 1** Spectral channel characteristics of SEVIRI in terms of central, minimum and maximum wavelength of the channels, and the main application areas of each channel

| Channel no. | Spectral band (μm) | Characteristics of spectral band (μm) | | | Main observational application |
|---|---|---|---|---|---|
| | | $\lambda_{cen}$ | $\lambda_{min}$ | $\lambda_{max}$ | |
| 1 | VIS0.6 | 0.64 | 0.56 | 0.71 | Surface, clouds, wind fields |
| 2 | VIS0.8 | 0.81 | 0.74 | 0.88 | Surface, clouds, wind fields |
| 3 | NIR1.6 | 1.64 | 1.50 | 1.78 | Surface, cloud phase |
| 4 | IR3.9 | 3.90 | 3.48 | 4.36 | Surface, clouds, wind fields |
| 5 | WV6.2 | 6.25 | 5.35 | 7.15 | Water vapor, high level clouds, atmospheric instability |
| 6 | WV7.3 | 7.35 | 6.85 | 7.85 | Water vapor, atmospheric instability |
| 7 | IR8.7 | 8.70 | 8.30 | 9.10 | Surface, clouds, atmospheric instability |
| 8 | IR9.7 | 9.66 | 9.38 | 9.94 | Ozone |
| 9 | IR10.8 | 10.80 | 9.80 | 11.80 | Surface, clouds, wind fields, atmospheric instability |
| 10 | IR12.0 | 12.00 | 11.00 | 13.00 | Surface, clouds, atmospheric instability |
| 11 | IR13.4 | 13.40 | 12.40 | 14.40 | Cirrus cloud height, atmospheric instability |
| 12 | HRV | Broadband (about 0.4–1.1 μm) | | | Surface, clouds |

**Table 2** AVHRR/3 channels characteristics

| Band no. | Band width (μm) | Resolution at Nadir (km) | Applications |
|---|---|---|---|
| 1 (visible) | 0.58–0.68 | 1.09 | Clouds and land surfaces cartography (day) |
| 2 (near IR) | 0.725–1.00 | 1.09 | Clouds and land surfaces cartography (day) |
| 3A (near IR) | 1.580–1.64 | 1.09 | Snow and ice detection |
| 3B (IR) | 3.550–3.93 | 1.09 | Clouds and sea surface temperature mapping (night) |
| 4 (IR) | 10.30–11.30 | 1.09 | Clouds and sea surface temperature mapping (night) |
| 5 (IR) | 11.50–12.50 | 1.09 | Sea surface temperature |

sponds to an angle of scanner rotation of 0.95 mrad. At this sampling rate, there are 1.362 samples per IFoV. A total of 2048 samples will be obtained per channel per Earth scan, which will span an angle of 55.4° from the Nadir (subpoint view).

Twice a day, the instrument provides images of the cloud cover over the entire world, and it also offers frequent images of the land and sea surfaces. The instrument is especially well suited for studying vegetation on a world scale, e.g., for the study of seasonal changes. It also allows monitoring sea surface temperatures and the ice covering extent.

### 2.3 General Operational Requirements

To receive in real time HRIT, HRPT, and APT satellite sensor data transmissions, a ground station is required. A block diagram of minimum ground station components is presented in Fig. 1.

The realized APT antenna consists of a Turnsteel omni-directional, circularly polarized beam fixed pointing straight up, while the HRPT and HRIT transmission formats use a microwave dish that is pointed at the satellite by our realized autotracker (described in Sect. 2.5).

The satellite signal level received by our ground station is lower and approximately equal to 4 mW; for this reason, we have realized a preamplifier.

In case of the APT acquisition mode, VHF II 137 MHz satellite signals are demodulated into audio tones (2400 Hz) by using a realized VHF II receiver, and afterward, a PC sound card adapted as analog to digital converter (ADC) block is used to convert the audio tones, which represent ana-

**Fig. 1** Essential hardware parts of MSG3 and NOAA19 satellites ground station used
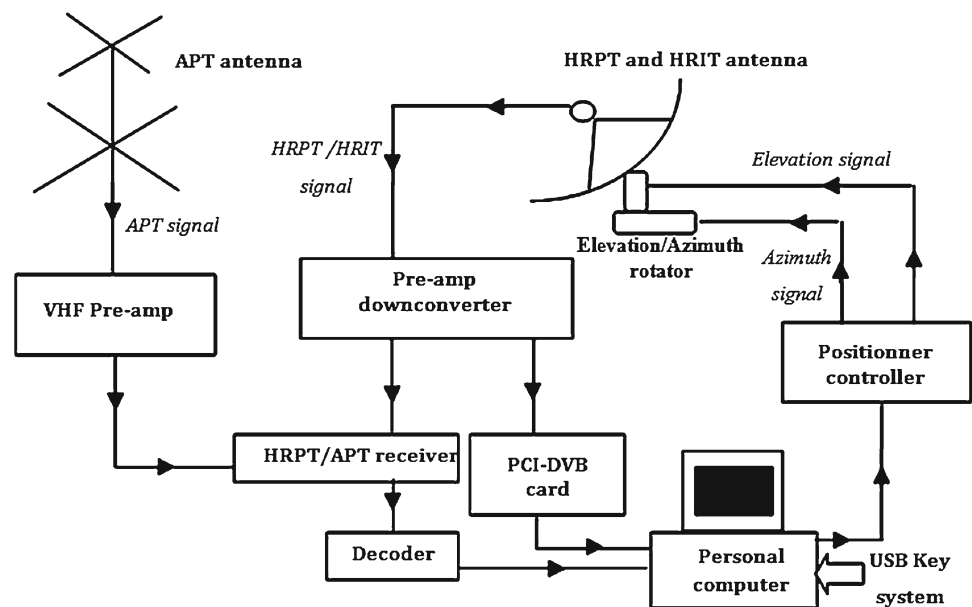


log voltage levels (generated by AVHRR sensor) into digital data entered and processed by the computer.

In case of the HRPT acquisition mode, the corresponding receiver demodulates the SHF (1.7 GHz) FSK-NRZ signal after frequency down-conversion to VHF II (150 MHz) by a LNB device [12].

Due to the higher frequencies and higher data rates for HRPT and HRIT transmissions, parabolic dish antennas are required to receive these data types. A parabolic dish reflector collects and concentrates the weak signals into a smaller receiving area referred to as a feed horn that is placed at the focal point of the reflector. This, and the use of electronic low-noise pre-amplification of the signal, makes it possible to receive noise-free transmissions.

The antenna system chosen for the HRPT signal is an L-band reflector associated with a circular cavity feed horn. It consists of a 1-m dish that provides adequate gain (around 24 dB) on pedestal a tripod with azimuth and elevation motors. The motorization is based on a heavy duty motorization. This provides 180° of freedom in elevation (maximum elevation velocity is 10°/s) and 450° of freedom in Azimuth (maximum azimuth velocity is 48°/s).

The pointing accuracy is approximately 4 % and the tracking accuracy is better than 0.2° for all satellite passes when the azimuth velocity is less than 0.5°/s. The dynamic requirements on the antenna control system are generated by the orbits of the satellites to be tracked and by the nature of the antenna mount. With an azimuth–elevation mount, it takes a very high azimuth velocity to track a low-altitude satellite passing close to the zenith, and a very low azimuth velocity to track a satellite pass as it comes up over the horizon.

The HRIT acquisition card is composed by a less expensive universal commercial PCI DVB satellite TV system connected with an USB key system. HRIT-MSG data from the European Organization for the Exploitation of Meteorological Satellites (EUMETSAT) are received via EUROBIRD 19 Est. satellite relay. Once the presence of HRIT signal in PCI DVB acquisition card is defined, EUMETSAT TechniSat software is used to decode it into a corresponding channel and save it as compressed image file on PC.

All compressed acquired data are opened and processed by using our MSGViewer (PC compatible) software written in C++ language.

### 2.4 Polar Satellite Passes Prediction

Since the NOAA satellites can cover a part of the same terrestrial area approximately four times per day but from different longitudes, the computer captures the data on to storage media for later processing. In either system, it is necessary to predict the satellites track both as paths above the Earth. For that, it is necessary to use an orbital prediction program and current orbital elements for the satellites to determine when they will be in direct visibility from our ground station; for this reason, we have developed quick software called PCNOAA_TRACK (Fig. 2). This application contains files with functions for calculating the position and rotational velocity of each operational satellite using the NORAD Simplified General Perturbations (SGP) 4 and Simplified Deep Space Perturbations (SDP) 4 routines, and from these the azimuth, elevation, range. Additional routines are also included in PCNOAA_TRACK for calculating the posi-
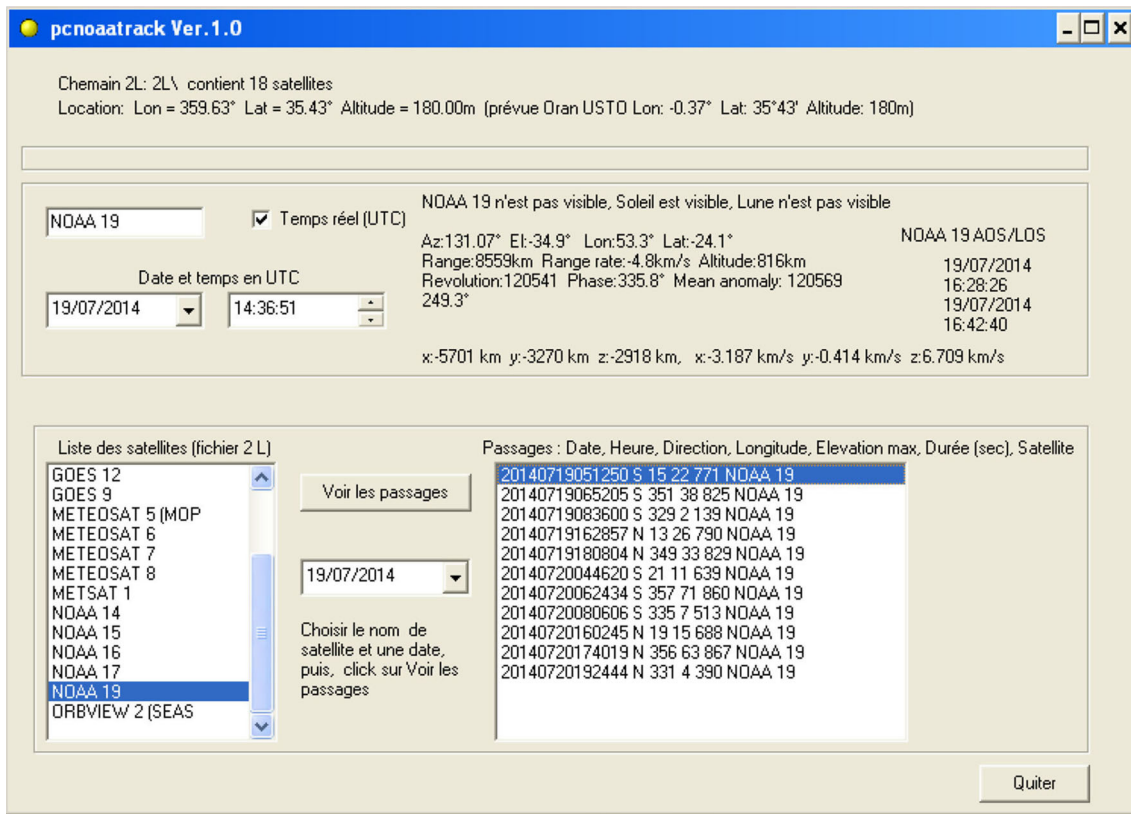
**Fig. 2** PCNOAA_TRACK software developed to predict NOAA19 pass and other satellites

tion of the sun and the illumination status and eclipse depth of the satellite. In the APT and the HRPT systems, the predictions inform the user when to have the system active and any slight error is generally not important.

The two-line element (TLE) is a format specified and used by NORAD and NASA. The TLE can be used directly by the SGP4 model (or one of the SGP8, SDP4, and SDP8 models). Orbital elements are freely distributed on NORAD website in text files. PCNOAA_TRACK works with the TLE orbital data files (resource.txt, stations.txt, and weather.txt contain the Keplerian orbit of each satellite). These files should be updated regularly, perhaps every month, because the SGP4 model has an error around 1 km at epoch and grows at 1–3 km per day. These data are updated frequently in NASA and NORAD sources due to this error. The original SGP model was developed by Yoshihide [13] refined by Hilton and Kuhlman [14] and was originally used by the National Space Surveillance Control Center (and later the United States Space Surveillance Network) for tracking of objects in orbit. The SDP4 model has an error of 10 km at epoch. The operating frequency and some technical information's for satellites are specified in the file TLEnotes.txt, which includes an explanation of the data format [15]. The format of data in TLEnotes.txt is documented in Fig. 3. A TLE is a data format used to convey sets of orbital elements that describe the orbits of Earth-orbiting satellites.

PCNOAA_TRACK can use the TLE to compute and predict the position of a satellite at a particular time and aim the dish antenna to this position by activating the autotracker.

SGP models apply to near-Earth objects with an orbital period of less than 225 min. SDP models apply to objects further from Earth or those with an orbital period greater than 225 min.

SGP4 orbital model takes into account the following perturbations:

- Atmospheric drag based on a static, non-rotating, spherically symmetric atmosphere,
- Fourth-order zonal geopotential harmonics,
- Spin-orbit resonance effects for synchronous and semi-synchronous orbits,
- Solar and lunar gravitational effects to the first order.

The latter two terms are less important for low-Earth orbit, for period less than 255 min (period for NOAA satellite series is about 102 min). Details of SGP4 and SDP4 are found in to [16,17].

To summarize, SGP4 uses a geopotential model of the fourth order described in Eq. (1).

$$V = -\frac{G \cdot M}{r} \left( 1 - \sum_{n=2}^{4} J_n \left( \frac{r_e}{r} \right)^n P_n \left( \sin \emptyset \right) \right) \qquad (1)$$

**Fig. 3** NASA/NORAD two-line elements description



where $V$ is the geopotential, $G$ is the gravitational constant, $M$ is the Earth's mass, $r$ is the Earth's mean radius, $\emptyset$ and $r_e$ are, respectively, the latitude and the radius of the observational point, $P_n$ is the normalized associated Legendre function, and $J_n$ represents the zonal terms.

This model takes into consideration:

- The equatorial pad of Earth ($J_2$),
- The pear form of Earth ($J_3$),
- An additional deviation ($J_4$).

It also models the atmospheric trail, which slows down satellites on their trajectories [18].

### 2.5 Satellite Autotracking System

In the HRPT part of the established system, however, we used the predictions to aim the dish antenna at the satellite as it passes above our receiving station, accuracy in the predictions and proper timing are essential. The HRIT reception needs a fixed 2-m-diameter dish. The HRPT system requires an autotracking motorized equipment.

The autotracker is an automatic positioner who consists of an azimuth–elevation motor controlled by using manual (using 4 digits keyboard) or automatic (using a serial Com PC port) positioning controller. Figure 4a shows the synoptic diagram of the autotracker realized in this research. Figure 4b presents the electronic scheme of the instrument, and the main device of the autotracker is the PIC16F876 microcontroller, including A/D converter, a bidirectional asynchronous serial port, in-circuit programming. With the open architecture and choice of design of our autotracker, it will allow others to implement a satellite antenna tracking interface at extremely low cost but simultaneously provide the highest versatility and compatibility of any PC. It uses a fairly standard PIC16F876 implementation. The only slightly novel approach is that if we choose an USB interface, then the FTDI USB/serial converter evaluation board is used. For

the RS-232 interface that we selected in this project, a standard MAX232 chip is used for level conversion. The FTDI USB/serial converter module is prefabricated using a standard 28 pin with DIL package. Although more expensive than using the 32 pin LQFP package, for ease of construction for the user the prefabricated module was used. The device is powered from the "Yaesu" rotator interface. Table 3 shows a list of connecting pins used by the autotracker circuit. The communication block ensures the contact between the PC (PCNOAA_TRACK software) and the microcontroller PIC16f876. The RS-232 connection receives the data from PC (PCNOAA_TRACK software) and sent to standardized voltages $+12/-12$ V, and the PIC16f876 receives these data on pins RC7/RX/DT with voltages 0/+5 V. The adaptation of the data is done using a circuit adapter of line (MAX232), which transforms the logical levels resulting from the numerical system (0/+5 V), in logical levels compatible with the standards RS-232 ($+12/-12$ V) and vice versa. The communication between the PC and the RS-232 connection is done under an EasyComm protocol. The control block allows the command of the antenna position compared to the satellite.

The antenna elevation and azimuth are recovered through pin 1 and 6, respectively, which are situated as DIN socket in the rear panel of Yaesu G-5500 rotator (controller block described in Fig. 5, Table 4). Each voltage from 2 to 4.5 VDC provided by the autotracker in pin 1 is corresponding to 0° to 180° in elevation of the antenna position, and each voltage from 2 to 4.5 VDC provided by the autotracker in pin 6 is corresponding to 0° to 450° in azimuth of the antenna position.

Analog to digital conversion is done on the level of RA0 and RA1 of PORTA of microcontroller; these two lines are configured as "input" of the converter. This one is the aim of our system; it ensures the correspondence between our PCNOAA_TRACK software and the Yaesu G-5500 rotator of the reception antenna. Moreover, the PORTC of microcontroller connects the control circuit through the lines (RC0–RC3), which are configured as "output." After hav-
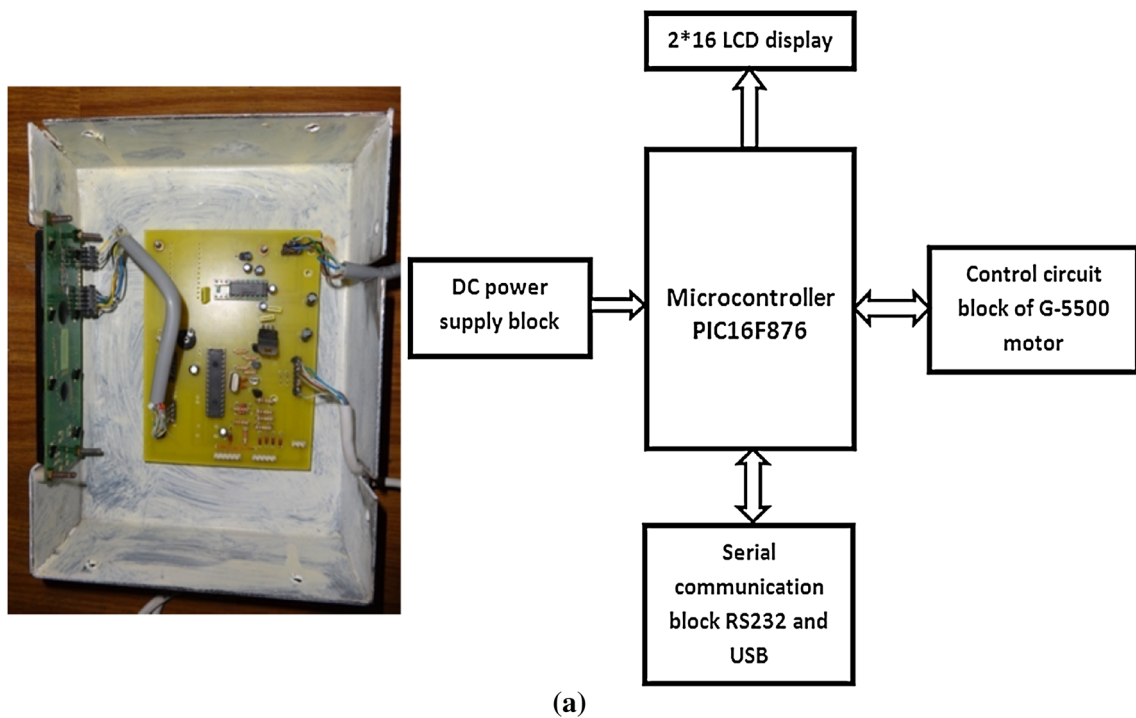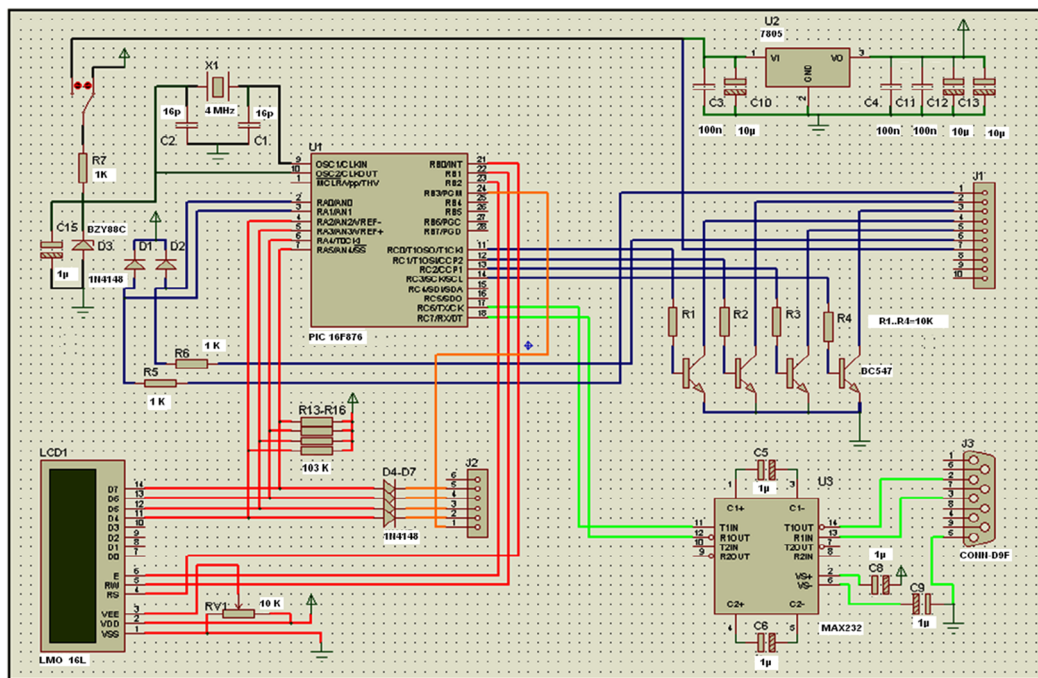
**Fig. 4** The autotracker realized: **a** synoptic diagram and photography of the autotracker, **b** electronic circuit of the realization

ing recovered the two analog potentials of elevation and azimuth, we can consider that the input condenser of the internal A/D converter module is charged, the converter then generates an digital result of this analog level via successive approximation. Once finished the analog/10-bit digital conversion, the digitized value is recorded in registers ADRESH and ADRESL. Then, the microcontroller will proceed to the comparison of these values compared to that provided by the PCNOAA_TRACK software. The difference between these two values will be sent through the RC0–RC3 pins of the PORTC like a command to control the position of the antenna. When one of these outputs is ON, transistor BC547 is saturated (the current of the collector is maximum), while it will be blocked when the output is OFF. Transistors (BC547)

**Table 3** List of connecting pins used in the autotracker circuit

| Pin | Number | Description |
|---|---|---|
| J1 | | To Yaesu 8 pins DIN |
| | 1 | Elevation |
| | 2 | Right |
| | 3 | Up |
| | 4 | Left |
| | 5 | Down |
| | 6 | Azimuth |
| | 7 | −13 V |
| | 8 | GND |
| J2 | 1–6 | LCD debugger header (optional) |
| J3 | | RS-232 (F) to PC |
| | 2 | RXD |
| | 3 | TXD |
| | 4 | DTR |
| | 5 | GND |
| | 7 | RTS |
| | 8 | CTS |
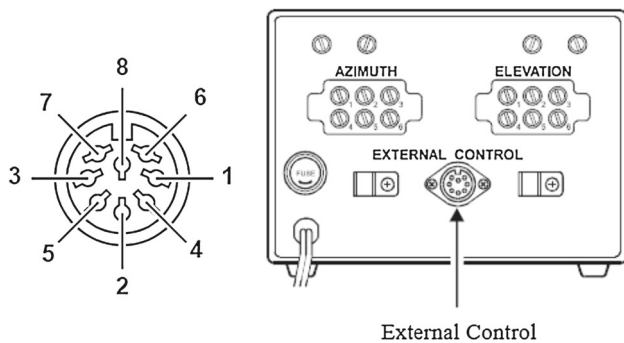


**Fig. 5** External control of the Yaesu command block: DIN socket connections

**Table 4** List of connecting pins used in the external DIN controller block of Yaesu G-5500 Rotator

| Pin number | Description |
|---|---|
| 1 | Provides 2–4.5 VDC corresponding to 0°–180° in elevation |
| 2 | Connect to Pin 8 to rotate right (clockwise) |
| 3 | Connect to Pin 8 to rotate down |
| 4 | Connect to Pin 8 to rotate left (counterclockwise) |
| 5 | Connect to Pin 8 to rotate up |
| 6 | Provides 2–4.5 VDC corresponding to 0°–450° in Azimuth |
| 7 | Provides 13–6 VDC at up to 200 mA |
| 8 | Common ground GND |

will change the potential in pins 2, 3, 4 and 5 of the DIN socket.

## 3 Results and Discussion

The realization of our ground station proceeded in two phases. Firstly, the complete APT and HRPT system was installed and tested in Laboratory of Analysis and Application of Radiations (LAAR). Two samples of manual (without autotracker) real-time acquisition images dates successively in June 22 and July 03, 2013 (acquired from NOAA19) are shown in Fig. 6.

Secondly, MSG3-HRIT system was effectively installed in February 05, 2014. Automatic satellite tracking tests with PCNOAA_TRACK software and the realized autotracker were carried out in 2014 during January and February at LAAR laboratory. Information concerning a geographic localization and latitude of our ground station is needed to initialize the autotracking operation. LAAR laboratory is situated in Faculty of Physics (Oran, USTOMB University, Algeria). It is located at latitude 35.43° North, longitude 0.37° West, and altitude around 50 m.

The downlink frequency for NOAA19 is 1698.0 MHz. The local oscillator for the down-converter used in our station has a frequency of 1557.0 MHz. The mean operation of the down-converter is to convert SHF (fs) signals from 1691.0 to 1707.0 MHz to VHFII ($f_c$) 134.0–150.0 MHz range, and the oscillator (Fig. 7) is accorded at fo around 1557.0 MHz. The frequency on the oscillator $f_c$ output is the difference between the input frequency fs and the oscillator fo frequency, i.e., $f_c = |f_s - f_o|$. Table 5 gives some examples about some satellite input/output frequencies treated by the down-converter. This means that the NOAA19 satellite signal is observable after down-conversion at frequency 141.0 MHz. Figure 8 shows a detailed scheme of the autotracking satellite system used. Figure 9a, b illustrates various sample response spectrums observed at LAAR laboratory. Figure 9a presents a reference spectrum with no satellite signal. Figure 9b presents a signal from HRPT NOAA19 at the down-conversion frequency of 141.0 MHz, detected in October 05, 2013.

Figure 10 presents, a sample of acquiring images from MSG3-SEVIRI sensor. The full images scan (12 channels) is acquired from MSG3 in June 09, 2014 at 11 h 15 min UTC. HRIT images are calibrated. This operation consists in converting infrared channels to thermal images by using the following method:

1. *Conversion from Counts to Radiances* the relation between the binary pixel value and the physical radiance is fully defined for each spectral band by the relation:

**Fig. 6** A sample of acquired images: **a** image APT received in June 22, 2014 at 13 h 20 min UTC (visible and infrared), **b** image HRPT received in July 03rd 2014 at 10 h 44 min UTC



**(a)**



**(b)**
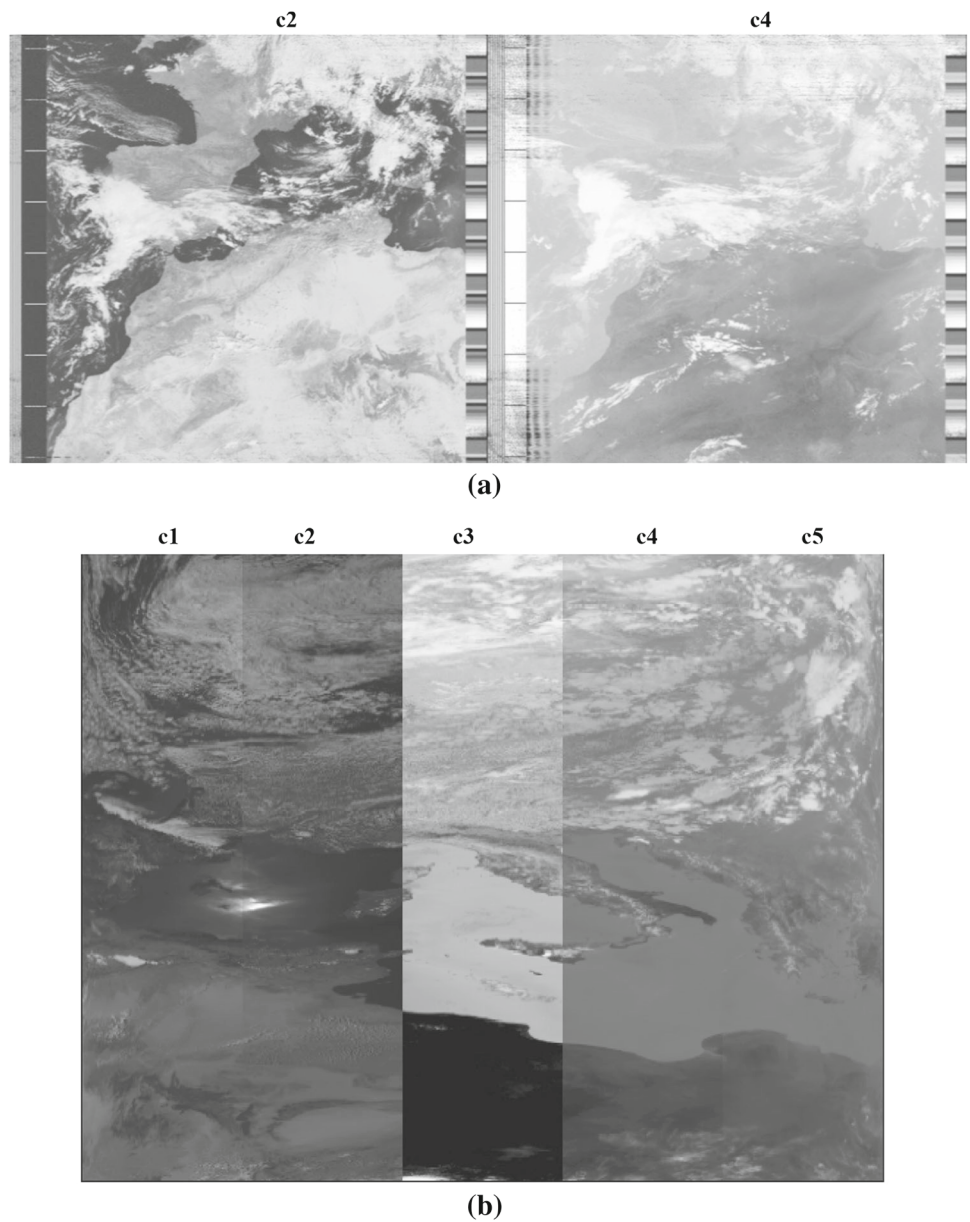
**Fig. 7** Synoptic scheme of the down-converter oscillator
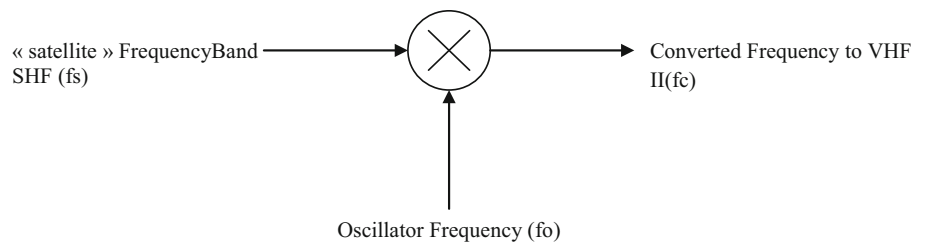


$$R = CAL\_offset + CAL\_slope.Count \qquad (2)$$

with:

$R$ is spectral radiance in m $\mathrm{Wm^{-2}\,sr^{-1}\,(cm^{-1})^{-1}}$,

*CAL_offset* is the offset constant between the pixel count and the physical radiance extracted either from the on-board calibration (for IR channels) or from other sources [e.g., SEVIRI Solar Channel Calibration (SSCC) for solar channels]. The units are $\mathrm{mW\,m^{-2}\,sr^{-1}\,(cm^{-1})^{-1}}$,

**Table 5** Some satellite input frequencies down-converted by pre-amp down-converter block

| Input frequency $f_s$ (MHz) | Oscillator frequency $f_o$ (MHz) | Output frequency $f_c$ (MHz) |
|---|---|---|
| 1691.0 | 1557.0 | 134.0 |
| 1694.5 | 1557.0 | 137.5 |
| 1698.0 | 1557.0 | 141.0 |
| 1707.0 | 1557.0 | 150.0 |

*CAL_slope* is the linear calibration coefficient extracted either from the on-board calibration (for IR channels) or from other sources [e.g., SEVIRI Solar Channel Calibration (SSCC)]. The units are mW m$^{-2}$ sr$^{-1}$ (cm$^{-1}$)$^{-1}$,
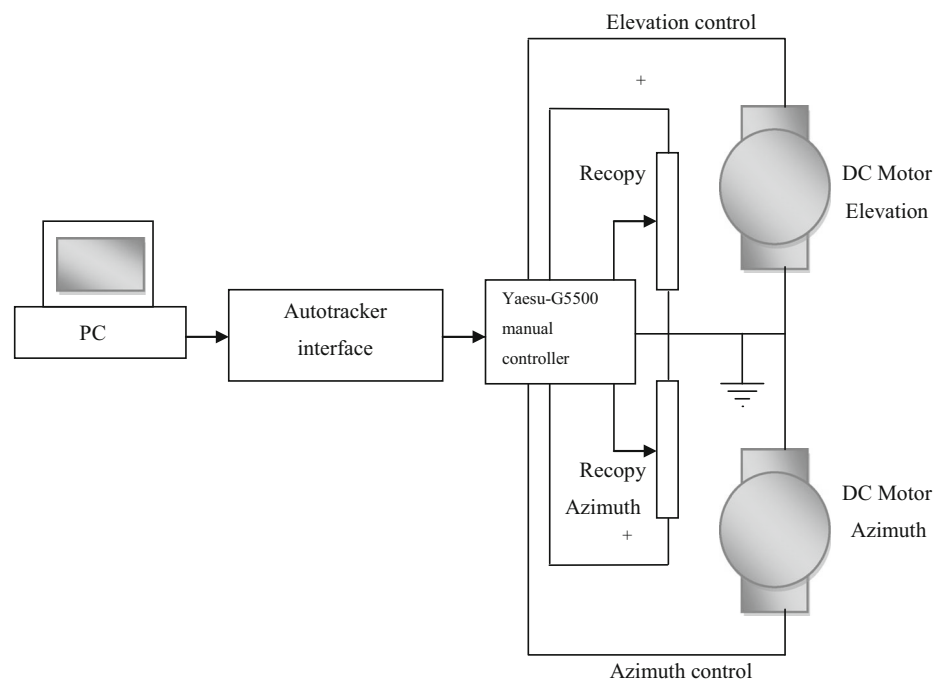*Count* is the binary pixel value (pixel count, between 0 and 1023).

2. *Conversion from Radiances to Brightness Temperatures* in the MSG, the following analytic relation between the equivalent brightness temperatures ($T_b$) and the SEVIRI radiances ($R$) is adopted:

$$T_b = \left[ C_2 \cdot v_c \left/ \log\left( \frac{C_1 \cdot v_c^3}{R} + 1 \right) - B \right] \right/ A \qquad (3)$$

with:

$C_1 = 1.19104\,10^{-5}$ mW m$^{-2}$ sr$^{-1}$ (cm$^{-1}$)$^{-4}$,
$C_2 = 1.43877$ K (cm$^{-1}$)$^{-1}$,
$v_c$ = central wavenumber of the channel, $A$ and $B$ are the coefficients depending to the type of MSG satellite.

In case of visible channels, the calibration operation allows converting each raw data to radiance [by using Eq. (2)] and then to terrestrial Albedo images. A simple way to calculate the reflectance for channels VIS0.6, VIS0.8 NIR1.6, and HRV is:

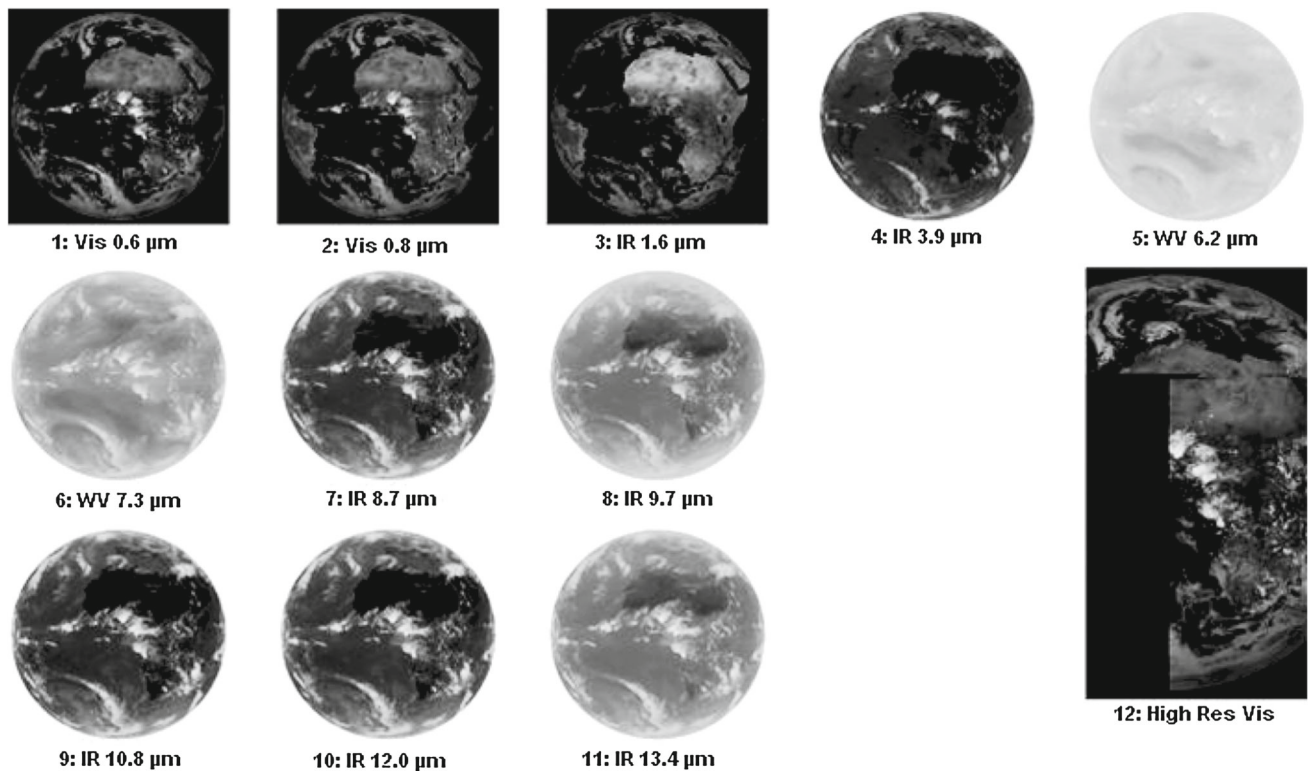$$REFL(i) = 100 \cdot R(i)/(TOARAD(i) \cdot \cos(TETA)) \qquad (4)$$

with:

$i$ is the number of Visible SEVIRI channel (1 = VIS0.6; 2 = VIS0.8; 3 = NIR1.6; 12 = HRV),
*REFL* is the reflectance (in %) for channel $i$,
$R$ is the measured radiance [in mW m$^{-2}$ ster$^{-1}$(cm$^{-1}$)$^{-1}$] for channel $i$,
*TOARAD* is the solar constant at top of the atmosphere [in mW m$^{-2}$ sr$^{-1}$ (cm$^{-1}$)$^{-1}$] for channel $i$,
*TETA* is the solar zenith angle (to be calculated from date, time, lat, lon); for twilight condition (i.e., $TETA > 80°$) TETA is set to 80° to avoid problems

$TOARAD\,(i = 1,\ VIS0.6) = 20.76/ESD**2$
$TOARAD\,(i = 2,\ VIS0.8) = 23.24/ESD**2$
$TOARAD\,(i = 3,\ NIR1.6) = 19.85/ESD**2$
$TOARAD\,(i = 12,\ HRV) = 25.11/ESD**2$

*ESD* is the Earth–sun distance (in Astronomical Units), which varies during the year according to the following equation:

**Fig. 8** Global scheme of the autotracking satellite system
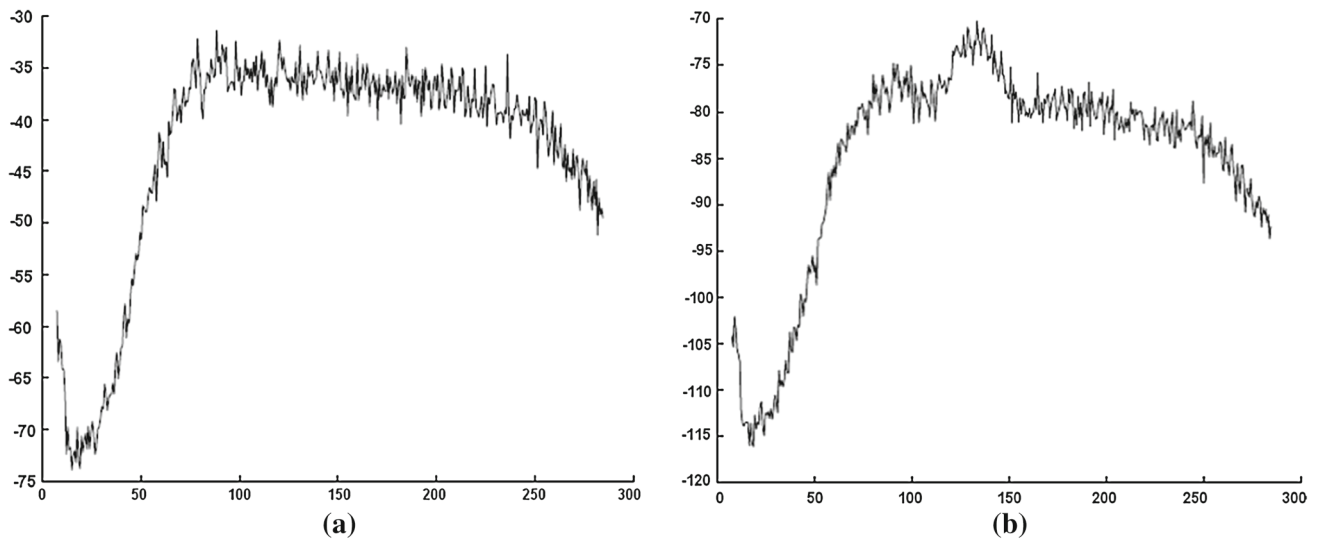
**Fig. 9** A sample spectra observed at LAAR laboratory by spectrum analyzer: **a** a reference spectrum with no satellite signal, **b** a signal from NOAA19 at down-converting frequency 141.0 MHz was detected in October 05, 2013



1: Vis 0.6 μm        2: Vis 0.8 μm        3: IR 1.6 μm        4: IR 3.9 μm        5: WV 6.2 μm

6: WV 7.3 μm        7: IR 8.7 μm        8: IR 9.7 μm

9: IR 10.8 μm        10: IR 12.0 μm        11: IR 13.4 μm        12: High Res Vis

**Fig. 10** A sample of one MSG3-HRIT scan acquired in June 12 2014 at 10 h 45 min UTC

$$ESD\,(JulianDay)$$
$$= 1.0 - 0.0167 \cdot \cos(2 \cdot \pi \cdot (JulianDay - 3)/365) \quad (5)$$

This algorithm is included in our MSGViewer software (Fig. 11).

Whereas Fig. 12a presents a sample of acquired Vis 0.6 SEVIRI-MSG3 channel before radiometric calibration process, which is raw data, Fig. 12b presents another one after the process, which is terrestrial Albedo. On the other hand, Fig. 12c, d presents raw and calibrated IR3.9 channels,
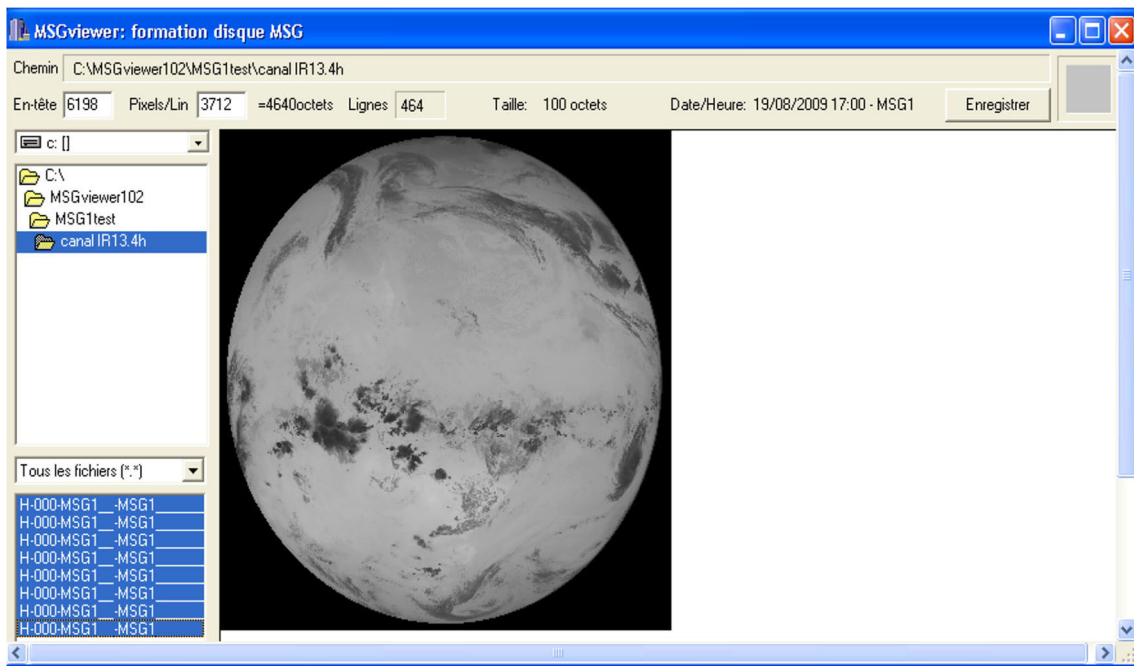
**Fig. 11** Main menu of MSGViewer software in full running

**Fig. 12** Radiometric correction results: **a** raw HRIT acquired Vis 0.6 μm image. **b** Terrestrial albedo image result. **c** Raw HRIT IR3.9 μm acquired image. **d** Brightness temperature image result
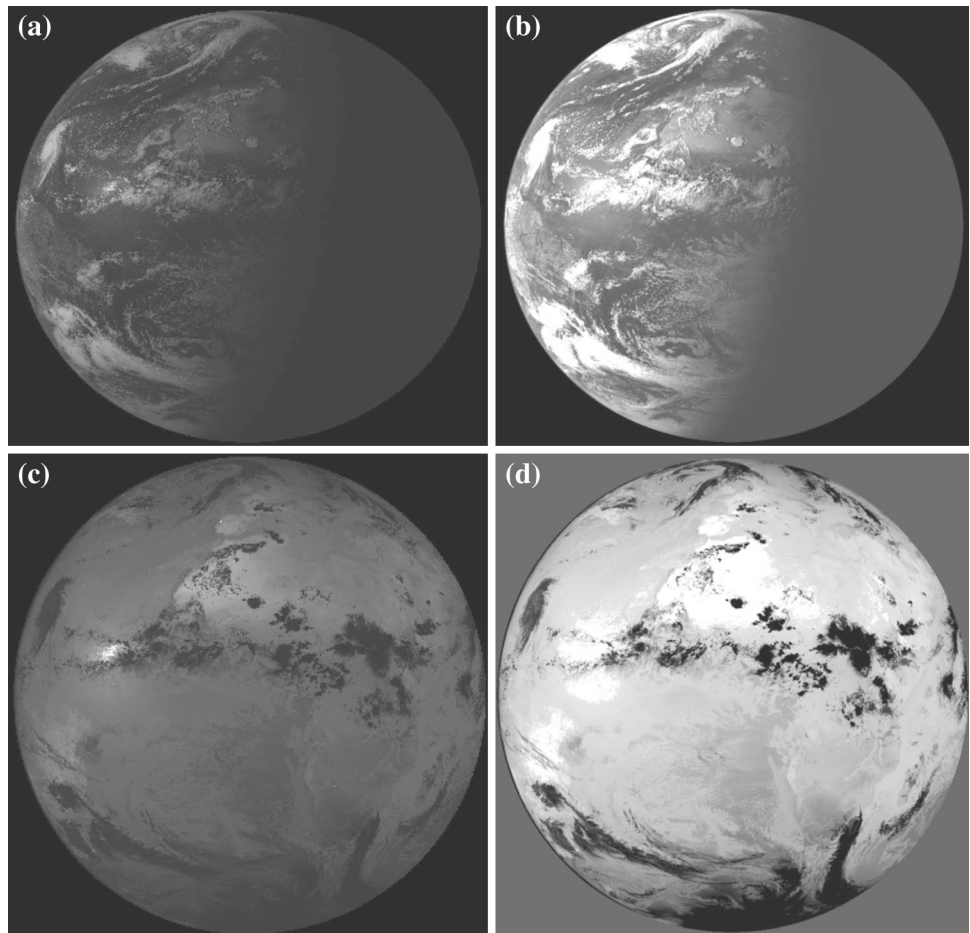
respectively. Each pixel in image result presents a brightness temperature count. Each calibration coefficient correspondingly associated with one satellite image is extracted from a prolog.txt file. All files are regrouped and transmitted to ground stations as a unique scan [19,20].

Calibration operation is considered as a preprocessing step in MSGViewer software. Some advanced processing levels are developed. For example, RGB combination operation shows a pixel color with coordinates $(x, y)$, denoted as $f(x, y)$, is a triplet $(r, g, b)$, where $r$, $g$, and $b$ are the intensities of the $R$ (for Red), $G$ (for Green), and $B$ (for Blue) components, respectively. RGB model means the three primary colors of the optical light, and it is composed of the color space representing an additive color system. RGB image composite is a technique to display the color imagery by using this three primary light color property [21].

Among processing and rendering methods for displaying MSG3-SEVIRI images, RGB composites by attributing 2–3 channels or channel combinations to individual color (RGB) beams provide a simple and fast type of classification by addition of RGB color intensities. RGB image composites retain natural texture of single-channel images. This method remains coherent in time and space, i.e., ideal for image sequence animation. It presents a fast technique for feature enhancement exploiting additive color scheme of RGB displays. Table 6 summarizes some combinations used to depict some thematic products.

After the application of a lat/lon mask and a "Rectangle Flat" geographic projection on each MSG3-SEVIRI image, we have applied some RGB combination standards in MSG3-SEVIRI images. Figure 13 presents the result of geographic projection and (R, G, B) = (3, 2, 1) combination. The projection operation allows correcting the panoramic error of each raw pixel and consists in transforming each pixel shape into a square of $3 \times 3\,\mathrm{km}^2$ in spatial resolution. Map transformations are referred to as projections because they are commonly visualized as geometric constructs. That is, we think of the map as a rectangle flat surface wrapped around a globe with lines emanating from points on the globe and "projected" onto the plane surface. It is important to note that not all map projections can be constructed in this manner. Map projections are specified as a set of equations giving $x$ and $y$ in terms of latitude and longitude. The way we wrap the rectangle around the globe determines the form of the equations. (R, G, B) = (3, 2, 1) combination commonly named 'true color combination' is essentially used to extract vegetation, some products such as sea water, bare soil and clouds, but limited to diurnal period of the day. Figure 14 presents another result of RGB (day) combination. We have used (R, G, B) = (2, 3, 4) to extract fog from another received image. Figure 15 shows the result of RGB (day) = (10–9, 9–7, $B = 9$) combination applied essentially to extract dust storms observed in the great Sahara of north

Africa, Delta Nile region, and the northeast region of the Arabian Golf.

On a purely comparative basis between our realized system and other existing stations like those described in Refs. [22,23], we can provide in real time multispectral satellite images (APT, HRPT, and HRIT) with less hardware part requirement, and hence, they are very much cheaper.

Currently, a large number of existing active earth observation satellites is a downlink transmission frequencies located in X-Band and L-Band. Our antenna auto tracking system can automatically tracks X-Band satellites like Moderate Resolution Imaging Spectroradiometer (MODIS)-TERRA and AQUA, Suomi-National Polar-orbiting Partnership (S-NPP), Joint Polar Satellite System-National Polar-orbiting Operational Environmental Satellite System (JPSS—NPOESS), and FengYun-3. To direct broadcast satellite images from X-Band transmission, we need to add and perform some parts of our station:

1. Changing a feed horn adapted to X-Band frequencies.
2. Introducing a low-noise amplifier (LNA) with X-band (7700–8500 MHz) input frequency with 50 dB minimum in Gain.
3. Including a Block Down Converter (BDC) with IF output frequency 800–1450 MHz and local oscillator frequency about 6950 MHz.
4. Adding an X-band programmable down-converter to convert 800–1450 to 720 MHz (IF filter Band width 120 MHz).
5. Adding for example a BPSK, QPSK, SQPSK, OQPSK high-rate demodulator compatible with the supported mode (Terra, Aqua, S-NPP, JPSS—NPOESS, FengYun-3) direct broadcast.
6. Developing some specifically softwares to decode and processing data acquired.

## 4 Conclusion

We presented in this paper the most technical directives for building and operating MSG3 and NOAA19 satellites receiving system. Remote-sensed data are gathered nearly in real time from SEVIRI and AVHRR sensors. They are applied for interesting combination results. This can give practical usefulness and expansion possibility for various topics related to remote sensing.

This research shows that receiving data in real time from the polar and geostationary satellites becomes relatively inexpensive proposal. The gathered data are useful in several remote sensing applications and are less expensive than commercially available datasets. The hardware and software required are modest when compared to a ground station for

**Table 6** Some standards RGB compositions applied in SEVIRI MSG images

| R, G, B composite | Applications | Period of the day |
|---|---|---|
| 03, 02, 01 | Vegetation, snow, smoke, dust, fog | Diurnal |
| 02, 03, 04 | Snow, fog | Diurnal |
| 02, 04, 09: | Clouds, convection, snow, fog, fires | Diurnal |
| 05–06, 04–09, 03–01 | Severe convection | Diurnal |
| 10–09, 09–04, 09 | Clouds, fog, contrails, fires | Nocturnal |
| 05–06, 08–09, 05 | Severe cyclones, jets, pv analysis | Diurnal and nocturnal |
| 10–09, 09–07, 09 | Dust, clouds (thickness, phase), contrails fog, ash, SO$_2$, low-level humidity | Diurnal and nocturnal |
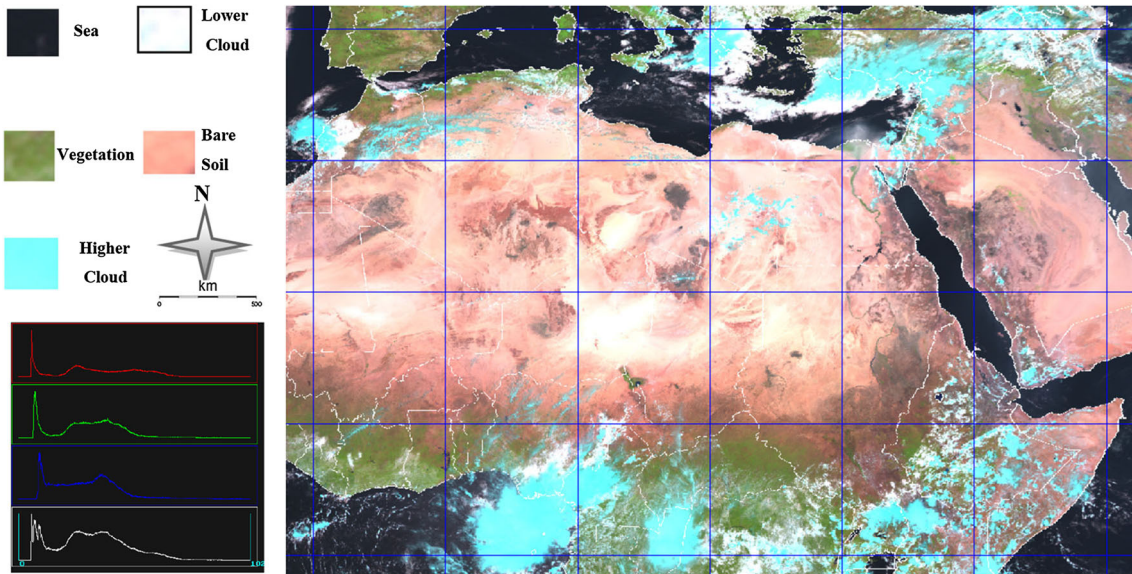


**Fig. 13** RGB day combination image: R = 3 (1.6 μm), G = 2 (0.6 μm), B = 1 (0.8 μm), image true color result
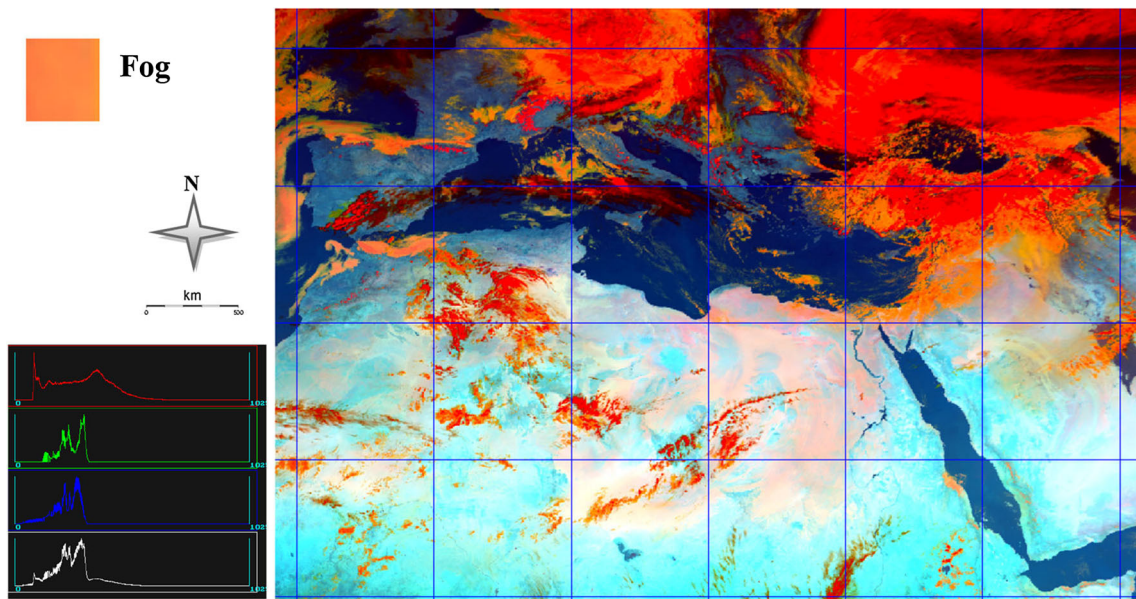


**Fig. 14** RGB day combination image: R = 2 (0.8 μm), G = 3 (1.6 μm), B = 4 (3.9 μm), extraction of Fog from MSG3-SEVIRI images
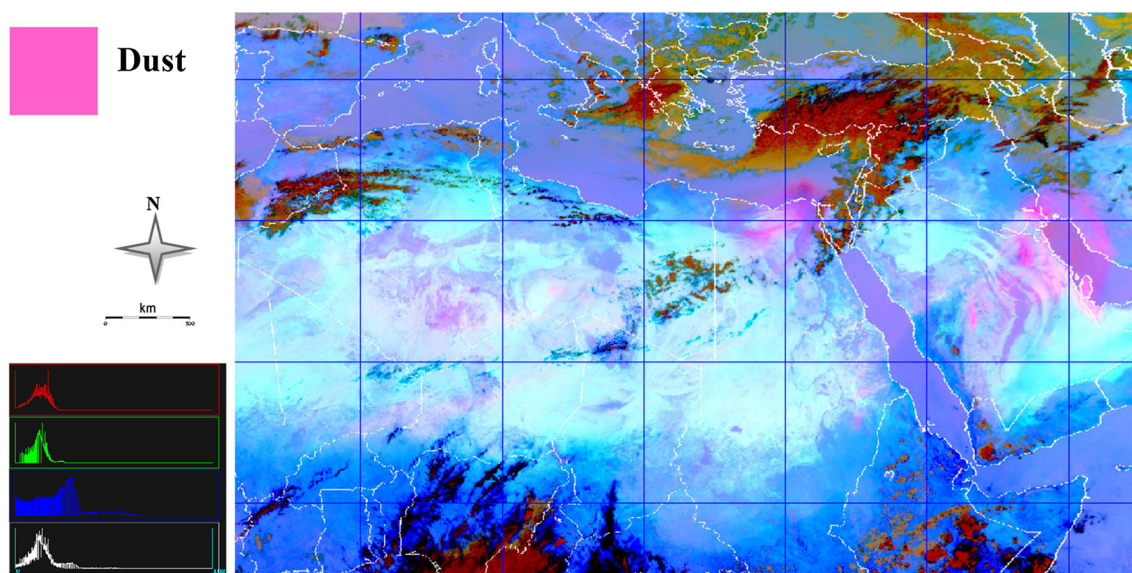
**Fig. 15** RGB day combination image: R = 10–9 (12–10.8 μm), G = 9–7 (10.8–8.7μm), B = 9 (10.8 μm), dust storm product extraction from acquired MSG3-SEVIRI images

other satellites. Approvals to this research, APT and HRPT data from NOAA19 satellite and HRIT data from MSG3 satellite are daily received. Some transformation operations used as combination between visible and infrared bands are applied for some collected database images. Diverse thematic products such as terrestrial Albedo, brightness temperature, vegetation, dust storm, and fog are reached, presented, and discussed here. We work at this moment to generate other thematic products using our image database and our developed software.

# References

1. Butt, M.J.; Waqas, A.; Iqbal, M.F.; Muhammad, G.; Lodhi, M.A.K.: Assessment of urban sprawl of Islamabad metropolitan area using multi-sensor and multi-temporal satellite data. Arab. J. Sci. Eng. **37**, 101–114 (2012)
2. Hadi, S.J.; Shafri, H.Z.M.; Mahir, M.D.: Factors affecting the eco-environment identification through change detection analysis by using remote sensing and GIS: a case study of Tikrit, Iraq. Arab. J. Sci. Eng. **39**, 395–405 (2014)
3. Abbasi, A.A.; Qureshi, M.S.: Estimating global, diffuse solar radiation for Chhor and validation with satellite-based data. Arab. J. Sci. Eng. **39**, 175–179 (2014)
4. Alothman, A.O.; Schillak, S.: Recent results for the Arabian plate motion using satellite laser ranging observations of Riyadh SLR station to LAGEOS-1 and LAGEOS-2 satellites. Arab. J. Sci. Eng. **39**, 217–226 (2014)
5. Viticchie, B.; Wagner, S.; Hewison, T.; Nain. J.; Gutierrez, R.; Müller, J.; Hanson, C.; Stone, T.: Lunar calibration of METEOSAT second generation SEVIRI solar channels. In: Abstract Brochure, 2013 Meteorological Satellite Conference, 19th American Meteorological Society (AMS) Satellite Meteorology, Oceanography, and Climatology Conference, Vienna, Austria, 16–20 Sept, p. 269 (2013)
6. Goodrum, G.; Kidwell, K.B.; Winston, W.: NOAA KLM User'S Guide with NOAA-N, -N', supplement, Section 3.1, Edition Jeffrey Robel. National Climatic Data Center (2009)
7. Waddell, J.E.: The state of coral reef ecosystems of the United States and Pacific Freely Associated States. In: NOAA Technical Memorandum NOS NCCOS 11. NOAA/NCCOS Center for Coastal Monitoring and Assessment's Biogeography Team, Silver Spring, p. 522 (2005)
8. Aminou, D.M.A.; Ottenbacher, A.; Jacquet, B.; Kassighian, A.: METEOSAT second generation: on-ground calibration, characterisation and sensitivity analysis of the SEVIRI imaging radiometer. In: Proceedings of SPIE 3750, Earth Observing Systems IV, vol. 3750, pp. 419–430 (1999)
9. Hadi, S.J.; Shafri, H.Z.M.; Mahir, M.D.: Factors affecting the eco-environment identification through change detection analysis by using remote sensing and GIS: a case study of Tikrit, Iraq. Arab. J. Sci. Eng. **39**, 395–405 (2014)
10. Kidwell, K.B.: NOAA polar orbiter data users guide. TIROS-N, NOAA-6, NOAA-7, NOAA-8, NOAA-9, NOAA-10, NOAA-11, NOAA-12, NOAA-13, and NOAA-14 (1997)
11. Hassini, A.; Belbachir, A.H.: AVHRR-NOAA and MODIS-Aqua/Terra data receiving and processing system. In: Schöning, M.J., Abdelghani, A. (eds.) Nanoscale Science and Technology (NS&T'12) Proceedings, Humboldt Kolleg, p. 83 (2012)
12. Zemaili, N. M.; Benbadji, N.; Hassini, A.; Belbachir, A.H.: Méthode d'étalonnage radiométrique des images satellitaires NOAA-HRPT. In: Troisièmes Journées d'Animation Scientifique du Réseau de Télédétection de l'AUF, JAS'09 Proceedings. USTHB, Algeirs, p. 435 (2009)
13. Yoshihide, K.: The motion of a close earth satellite. Astron. J. **64**, 367–377 (1959)
14. Hilton, C.G.; Kuhlman, J.R.: Mathematical Models for the Space Defense Center. Philco-Ford. Publication No. U-3871, pp. 17–28 (1966)
15. Hassini, A.; Benabadji, N.; Belbachir, A.H.: Acquisition and treatment of MSG satellite images. In: 5th International Conference on Sciences of Electronic, Technologies of Information and Telecommunications, SETIT 2009 Proceedings, Tunisia, p. 563 (2009)

16. Hoots, F.R.; Roehrich, R.L.: Space track report no. 3: models for propagation of NORAD element sets. Peterson: Aerospace Defense Command. United States Air Force, pp. 1–79 (1980)

17. Shenggang, L.; Chao,H.; Shaokai, W.; Qinqin, L.: Data warehouse design for Earth observation satellites. In: 2012 International Workshop on Information and Electronics Engineering, Procedia Engineering, vol. 29, pp. 3876–3882 (2012)

18. Bak, T.: Spacecraft attitude determination—a magnetometer approach, 2nd edn. Ph.D. thesis, Department of Control Engineering, Aalborg University, Aalborg Ø, p. 188 (1999)

19. Hassini, A.; Benabdelouahed, F.; Benabadji, N.; Belbachir, A.H.: Active fire monitoring with level 1.5 MSG satellite images. Am. J. Appl. Sci. **6**(1), 157–166 (2009)

20. Benkahla, N.; Hassini, A.: Identification of terrestrial vegetation by MSG-SEVIRI radiometer and follow-up of its temporal evolution. In: Amine, A.; Otmane, A.M.; Bellatreche, L. (eds.) Studies in Computational Intelligence Series, vol. 488, pp. 305–314. Springer, Berlin (2013)

21. Hassini, A.; Déjean, S.; Benabadji, N.; Hassini, N.; Belbachir, A.H.: Forest fires smoke monitoring from sea-viewing wide field-of view sensor images. Opt. Appl. **38**(4), 737–754 (2008)

22. Nordin, M.S.; Abdul Aziz, F.: Ground receiving station (GRS) of UMS—receiving and processing the electromagnetic wave data from satellite. J. Nucl. Relat. Technol. **4**, 199–208 (2007)

23. Friedt, J.M.: Satellite image eavesdropping: a multidisciplinary science education project. Eur. J. Phys. **26**, 1–16 (2005)